Decaying grid turbulence in a rotating stratified fluid

Olivier Praud, Joël Sommeria, Adam M. Fincham

Decaying grid turbulence in a rotating stratified fluid

By OLIVIER PRAUD†, JOEL SOMMERIA AND ADAM M. FINCHAM‡

Laboratoire des Ecoulements Géophysiques et Industriels (LEGI) CNRS-UJF-INPG, Coriolis, BP53, 38041 Grenoble, cedex 9, France

Rotating grid turbulence experiments have been carried out in a stably stratified fluid for relatively large Reynolds numbers (mesh Reynolds numbers up to 18 000). Under the combined effects of rotation and stratification the flow degenerates into quasi-horizontal motions. This regime is investigated using a scanning imaging velocimetry technique which provides time-resolved velocity fields in a volume. The most obvious effect of rotation is the inhibition of the kinetic energy decay, in agreement with the quasi-geostrophic model which predicts the absence of a direct energy cascade, as found in two-dimensional turbulence. In the regime of small Froude and Rossby numbers, the dynamics is found to be non-dissipative and associated with a symmetric and highly intermittent vertical vorticity field, that displays k_h^{-3} energy spectra. For higher Rossby numbers, fundamental differences with the quasi-geostrophic model are found. A significant decay of kinetic energy, which does not depend on the stratification, is observed. Moreover, in this regime, although both cyclones and anticyclones are initially produced, the intense vortices are only cyclones. For late times the flow consists of an assembly of coherent interacting structures. Under the influence of both rotation and stratification, they take the form of lens-like eddies with aspect ratio proportional to f/N.

1. Introduction

Turbulence in the atmosphere and oceans is generally influenced by planetary rotation and density stratification. Both effects tend to produce highly anisotropic flow structures, with quasi-horizontal velocity fields. However, while rotation alone produces columnar eddies aligned with the axis of rotation, stratification produces layered eddies of short vertical extent. The turbulence dynamics under these two antagonistic effects is still not fully understood.

The present paper reports an experimental study of freely decaying grid turbulence in the presence of both stratification and rotation. The experiments were performed on the 'Coriolis' turntable in Grenoble, whose large scale (13 m in diameter) allows the production of turbulence dominated by stratification and rotation effects. Stratification is characterized by the Brunt–Väisälä frequency N and rotation by the Coriolis parameter f. The ratio f/N is varied in the range $0 < f/N < 1.2$, to study the competition between these two effects. The case with pure stratification ($f = 0$) has been

† Present address: I.M.F.T., Allíe du Prof. Camille Soula 31400 Toulouse, France.

‡ Present address: Dept of Aerospace and Mechanical Engineering, University of Southern California, RRB 101, 854 W 36th Place, Los Angeles, CA 90089, USA.

reported earlier (Praud, Fincham & Sommeria 2005), and here we focus on the influence of rotation. In the non-rotating stratified regime, the flow splits into multiple layers with pancake eddies. Riley, Metcalfe & Weissman (1981) and Lilly (1983) have suggested that, in the limit of small Froude number (strong stratification), stably stratified turbulence could obey two-dimensional dynamics. However, numerical (see Herring & Metais 1989; Smith & Waleffe 2002) and experimental (see Fincham, Maxworthy & Spedding 1996; Praud *et al.* 2005) studies have shown that the shear between layers increases with stratification, such that the global energy dissipation remains close to that of ordinary three-dimensional turbulence. This is in stark contrast with the dynamics of two-dimensional turbulence, where in the limit of large Reynolds numbers there is no energy dissipation.

When turbulence is subjected to rotation alone, energy transfer toward the small scales is severely reduced, so that inertial waves and two-dimensional eddies thus coexist for a long time. The tendency towards two-dimensionalization has been extensively studied in homogeneous isotropic turbulence using theoretical and numerical simulations, both DNS (direct numerical simulations) and LES (large-eddy simulations) (see Bardina, Ferziger & Rogallo 1985; Bartello, Metais & Lesieur 1994; Cambon, Mansour & Godeferd 1997; Smith & Waleffe 1999; Cambon, Rubinstein & Godeferd 2004). It has been found that nonlinear interactions between inertial waves, which initiate the transition from three-dimensional to two dimensional turbulence do not lead to a truly two-dimensional dynamics (Cambon *et al.* 1997). In particular, it does not exhibit the classical inverse energy cascade (Smith & Waleffe 1999). When boundary effects constrain inertial waves, the tendency toward two dimensionalization is favoured. This is the case for a fluid confined between two plates perpendicular to the axis of rotation. Then the only source of energy decay is the Ekman friction at the bounding walls. The effect of vertical confinement was numerically investigated by Godeferd & Lollini (1999).

In addition, rotating turbulence is associated with the emergence of persistent columnar vortices aligned with the rotation axis. Nevertheless, they should not be considered as exact two dimensional vortices. The creation of such organized structures has been observed in various experiments, first by de Verdiere (1980), and in numerical simulation of forced rotating turbulence (Smith & Waleffe 1999). In the case of unforced initially three-dimensional isotropic rotating turbulence, the spontaneous generation of such vortices is enforced by the presence of solid boundaries which vertically confine the flow (Godeferd & Lollini 1999). The Ekman pumping, induced by the presence of horizontal walls, appears to be essential in generating coherent vortices as these features are not obtained in the unforced homogeneous case.

For large rotation rates (small Rossby numbers Ro), intense vortices of both signs emerge in a symmetric way (Hopfinger, Browand & Gagne 1982). At moderate rotation rates ($Ro \sim O(1)$), by contrast, axial coherence is observed preferentially for cyclonic vortices, for which local rotation adds to the background rotation, while the anticyclones tend to remain three dimensional or instable (Hopfinger *et al.* 1982; Godeferd & Lollini 1999; Smith & Waleffe 1999). For instance, the experiments of Hopfinger *et al.* (1982) have clearly shown the presence of intense cyclonic vortices in a background of weaker anticyclonic vortices.

The case of rapid rotation combined with a strong stratification is usually called geostrophic turbulence. It is the typical regime for meso-scale atmospheric and oceanic motion. An analytical theory has been proposed by Charney (1971), using the quasi-geostrophic model, valid in the limit of small Froude and Rossby numbers. Charney noted a formal analogy with two dimensional turbulence, and on the basis of inviscid

conservation laws, he proposed the occurrence of an inverse cascade of total energy and a direct cascade of potential enstrophy (squared potential vorticity). He assumed three-dimensional isotropy of the energy and potential enstrophy spectra, once the vertical coordinate has been rescaled by N/f, according to the invariance of the quasi-geostrophic equations under vertical stretching with a corresponding change in N/f. Herring (1980) largely confirmed Charney's conjectures in the framework of a statistical closure model. The dynamics is then completely dominated by the potential vorticity modes and exhibits the inverse cascade of energy and the forward cascade of potential enstrophy.

This quasi-geostrophic approximation, however, discards some physical effects, such as the interaction of turbulence with internal inertio-gravity waves. The various resonant interactions and energy transfer have been investigated by Bartello (1995) and Smith & Waleffe (2002). The results of Smith & Waleffe (2002) suggest that the quasi-geostrophic dynamics is valid for small Froude number ($Fr \ll 1$) in the domain $1/2 \leqslant f/N \leqslant 2$. A common result of the various studies is the general tendency of energy transfer to slow modes when the Rossby or Froude numbers are small. Therefore, under the joint effects of rotation and stratification, energy is protected from dissipation, as the direct energy cascade to small scales is severely reduced. Furthermore Ekman friction is limited by stratification to regions near the boundaries, with weak influence in the interior.

Ageostrophic effects such as wave–vortex interactions could however play a crucial role in rotating stratified turbulence. Babin, Mahalov & Nicolaenco (1998) suggested that these wave–vortex interactions contribute to the nonlinear adjustment to the geostrophic state. Asymmetry between cyclones and anticyclones is also due to effects beyond the quasi-geostrophic approximation (see Hakim, Snyder & Muraki 2002). These effects involve interactions of different space and time scales and may be difficult to capture in numerical computations. A recent review on the effect of stratification and rotation on turbulence flows can be found in Cambon (2001).

Because of practical constraints, few experimental studies of turbulence in the presence of stratification and rotation have been performed. Linden, Boubnov & Dalziel (1985) described the response of a rotating stratified fluid to forcing produced by horizontal sources and sinks. In these experiments, the flow appears to evolve with a balance between an inverse cascade produced by the two-dimensionality of the flow and a cascade due to baroclinic instability. The authors also noticed the development of an asymmetry between cyclones and anticyclones: for $f/N > 2$ a predominance of cyclonic vorticity is observed.

The formation of coherent structures is a generic feature of the collapse of turbulence regions in rotating stratified fluids. They are lenticular with characteristic aspect ratios of order f/N, and the vertical and horizontal scales adjust, such that the effects of stratification and rotation balance. Baroclinic and internal barotropic instabilities constrain the vortex shape. This natural tendency to form coherent structures has been observed and extensively discussed by McWilliams (1984, 1989, 1990) and McWilliams, Weiss & Yavneh (1999). Numerical simulations have shown that the presence of such intermittent vortices could modify classical statistical predictions such as the enstrophy cascade process, leading to steeper energy spectra. For late times, the dynamics of the flow is controlled by the vortex interactions.

The present paper focuses on the combined influence of rotation and stratification on the dynamics of turbulence, including kinetic energy decay, three-dimensional structure of the flow and the emergence of coherent vortices. For small Rossby numbers, the results are found to be consistent with the quasi-geostrophic model, in particular

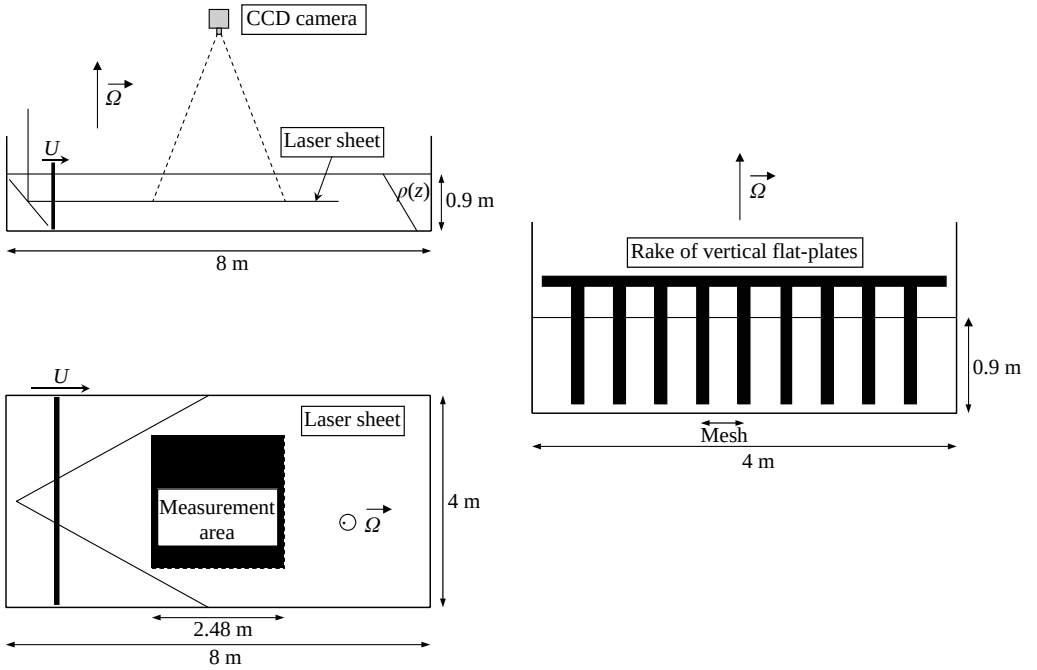

FIGURE 1. Side, top and front views of the experimental set-up.

the very weak energy decay, the emergence of coherent vortices which are geostrophically balanced and a strongly intermittent vertical vorticity field, statistically symmetric with respect to cyclones and anticyclones. For moderate rotation rates, departure from this model is observed: the flow is dominated by cyclonic vortices which appear stronger and more barotropic, whereas the anticyclones remain fragmented.

The paper is organized as follows. In § 2 the experimental apparatus and the measurement technique are described; the inhibition of the decay of kinetic energy is discussed in § 3. A general description of the flow, including the length-scale evolution and a discussion of the antagonistic effects of rotation and stratification is given in § 4. The emergence of coherent vortices and the intermittent and symmetric properties of the vorticity field are commented on in § 5. Finally the conclusion is presented in § 6.

2. Experimental set-up and procedure

2.1. *Experimental apparatus*

The experiments were performed in a closed rectangular channel (8 m × 4 m) constructed on the 'Coriolis' rotating platform (a circular tank with diameter 13 m) see figure 1. The axis of rotation is vertical to within 3×10^{-6} rad, and the angular velocity is constant within a precision of $\Delta\Omega/\Omega < 10^{-4}$. The average water depth is 0.9 m (the variations due to the parabolic free surface are less than 2 cm). The whole tank is filled with water to avoid leaks from the channel. The tank is linearly stratified with common salt by diluting an ultrasonically maintained constant-head filling flow with a prescribed flux of brine provided by a computer-controlled volumetric pump. The water temperature is stabilized and controlled to better than 1 °C, such that density variations associated with temperature fluctuations can be neglected. The density stratification is measured before and after each experiment by a profiling conductivity probe that moves at 2 cm s^{-1}.

The turbulence is generated by towing a rake of vertical flat plates of width $W = 10\,\mathrm{cm}$ and mesh spacing $M = 45\,\mathrm{cm}$, at a constant speed U along the full length of the channel. The rake is hung from a carriage that moves above the free surface and its displacement is driven through a computer-controlled DC motor, ensuring good repeatability of the experiments. The velocity of the rake increases linearly from 0 to U and, at the end of the motion, decreases linearly back to zero. The acceleration and deceleration are chosen to minimize the generation of internal gravity waves by the accumulation of the fluid between the rake and the endwalls of the channel. A set of vertical plates is used instead of a standard grid with the objective of minimizing internal wave generation and avoiding selection of a particular vertical length scale. The plates were chosen instead of rods, as they provide a well-defined separation point that is generally independent of the Reynolds number. When generating turbulence by means of this rake we introduce a maximum of kinetic energy into the horizontal modes which minimizes dissipation of energy due to the initial three-dimensional turbulence state. This helps to maintain the energy entering the rotating stratified turbulence state, which is then attained at higher Reynolds numbers.

A high-resolution scanning digital particle image velocimetry system was used in these experiments, as described by Fincham & Spedding (1997) and Fincham (1998). This system provides the horizontal velocity projection in a volume ($2.48\,\mathrm{m} \times 2.48\,\mathrm{m} \times 0.5\,\mathrm{m}$), with relative precision about 2 %. The spatial derivatives along x, y and z are obtained by differentiation of the velocity data. Turbulence statistics are obtained within this volume as a function of time, whose origin is chosen when the rake is located at the centre of the measurement area. The measurement volume is centred in the channel to avoid boundary effects. Figure 1 shows the experimental facility and the orientation of the measurement area. More details about the experimental techniques are provided in Praud *et al.* (2005) and Praud & Fincham (2005).

2.2. *Scales and parameters*

We denote by l_h a horizontal length scale and by V a typical horizontal velocity. Since the motion quickly becomes quasi-horizontal, we choose l_h/V for the advective time scale. The buoyancy time scale based on the mean stratification is $1/N$ where $N = \sqrt{-(g/\rho_0)(\partial\rho/\partial z)}$ is the Brunt–Väisälä frequency. The ratio of these two time scales defines a horizontal Froude number which compares buoyancy effects to inertia and therefore measures the relative importance of stratification:

$$Fr_h = V/l_h N. \tag{2.1}$$

The relative importance of rotation is similarly characterized by the Rossby number:

$$Ro = V/l_h f \tag{2.2}$$

where $f = 2\Omega$ is the Coriolis parameter (Ω is the background angular rotation rate); the vertical axis is chosen to be aligned with the axis of rotation and the mean density gradient, $\partial\rho/\partial z$. The ratio f/N characterizes the relative importance of rotation and stratification.

From the main control parameters, which are the mesh size M, the velocity of the rake U, the Coriolis parameter f and the Brunt–Väisälä frequency N, we define the initial Froude number, Fr_M, Rossby number, Ro_M and Reynolds number Re_M:

$$Fr_M = \frac{U}{MN}, \qquad Ro_M = \frac{U}{Mf}, \qquad Re_M = \frac{UM}{\nu}, \tag{2.3}$$

Exp	U (cm s^{-1})	Re_M	N(s^{-1})	f (s^{-1})	Fr_M	Ro_M	f/N
ba	0.5	2250	0.52	0	0.02	–	0
bb	1	4500	0.52	0	0.04	–	0
bc	2	9000	0.52	0	0.09	–	0
bd	4	18000	0.52	0	0.17	–	0
be	8	36000	0.52	0	0.34	–	0
fa	0.5	2250	0.52	0.08	0.02	0.14	0.15
fb	1	4500	0.52	0.08	0.04	0.28	0.15
fc	2	9000	0.52	0.08	0.09	0.56	0.15
fd	4	18000	0.52	0.08	0.17	1.13	0.15
da	0.5	2250	0.52	0.16	0.02	0.07	0.3
db	1	4500	0.52	0.16	0.04	0.14	0.3
dc	2	9000	0.52	0.16	0.09	0.28	0.3
ea	0.5	2250	0.52	0.32	0.02	0.04	0.6
eb	1	4500	0.52	0.32	0.04	0.07	0.6
ec	2	9000	0.52	0.32	0.09	0.14	0.6
ed	4	18000	0.52	0.32	0.17	0.28	0.6
ia	0.5	2250	0.26	0	0.04	–	0
ib	1	4500	0.26	0	0.09	–	0
ic	2	9000	0.26	0	0.17	–	0
id	4	18000	0.26	0	0.34	–	0
ha	0.5	2250	0.26	0.08	0.04	0.14	0.3
hb	1	4500	0.26	0.08	0.09	0.28	0.3
hc	2	9000	0.26	0.08	0.17	0.56	0.3
hd	4	18000	0.26	0.08	0.34	1.13	0.3
ga	0.5	2250	0.26	0.32	0.04	0.04	1.2
gb	1	4500	0.26	0.32	0.09	0.07	1.2
gc	2	9000	0.26	0.32	0.17	0.14	1.2
gd	4	18000	0.26	0.32	0.34	0.28	1.2

TABLE 1. Recapitulation of the different experiments performed with the appropriate initial parameters.

where ν is the mean kinematic viscosity, i.e. the viscosity of the salt solution at mid-depth of the tank (viscosity varies by 5.6 % with depth in the most stratified case, with $\delta\rho/\rho = 2.5\,\%$). Table 1 summarizes the different experiments performed and figure 2 represents them in a diagram of non-dimensional parameters. The horizontal axis represents the purely stratified cases without rotation, while the vertical axis represents homogeneous fluid cases. For the experiments, stratification dominates over rotation ($f/N < 1$) for all cases except ga, gb, gc, gd, for which $f/N = 1.2$.

More relevant non-dimensional parameters can be defined from the turbulent velocity and horizontal integral length scale, $Re = Re_M u^* L_h^*$, $Ro = Ro_M u^*/L_h^*$ and $Fr = Fr_M u^*/L_h^*$, where u^* and L_h^* are respectively the dimensionless turbulent velocity, given by the square root of the measured kinetic energy (see figure 4 below and the dimensionless horizontal integral scale given by (4.1) below. At $t^* = tU/M = 10$, which correspond roughly to the beginning of the well-established turbulent decay, $u \sim 0.15U$ and $L_h \sim 1.6M$; thus, in comparison with definitions (2.3) the Reynolds number should typically be divided by 5, and the Froude and Rossby numbers by 10. As the velocity decreases and the length increases, the Reynolds, Froude and Rossby numbers decrease with time.

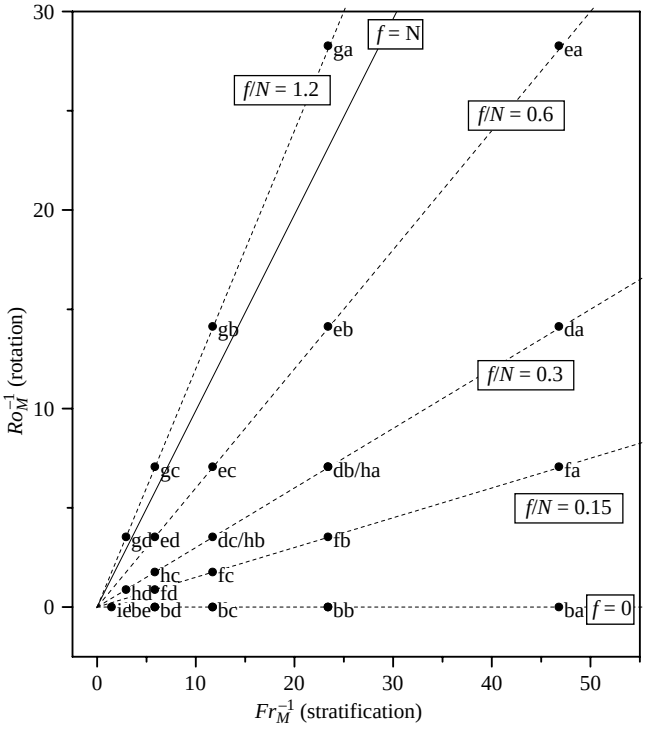

FIGURE 2. Diagram of the different experiments as a function of their initial non-dimensional parameters, based on the grid mesh M and velocity U (the corresponding non-dimensional parameters based on the turbulent velocity and integral scale are about 10 times lower).

Since the Froude number is initially small for all the experiments, the flow constantly evolves in conditions of strong stratification ($Fr_h \ll 1$). In the absence of rotation, the vertical Froude number, based on a vertical length scale, can be initially of order 1 (even if Fr_h is very small) as already observed by Praud *et al.* (2005), Godeferd & Staquet (2003) and Billant, Chomaz & Huerre (2000). However, due to the decay of turbulence, the vertical Froude number rapidly decreases to values much smaller than unity. When rotation is present the ratio of the horizontal to the vertical Froude numbers, given by the ratio of the vertical to the horizontal length scales, is thus proportional to f/N. During this decay, the ratio f/N does not change, that is, the evolution of each experiment takes place along a line of constant f/N (see figure 2) with the values of Fr^{-1} and Ro^{-1} increasing in time.

3. Kinetic energy and energy spectra

3.1. *Quasi-horizontal motion*

Immediately after the passage of the rake, different initial behaviours are observed. For low towing speeds, the initial wake is laminar with quasi-horizontal motions; while for higher towing speeds, three-dimensional turbulence is observed directly behind the rake. This turbulence soon collapses into quasi-horizontal motion. In this regime, individual coherent vortices emerge and their subsequent evolution can be accurately tracked.

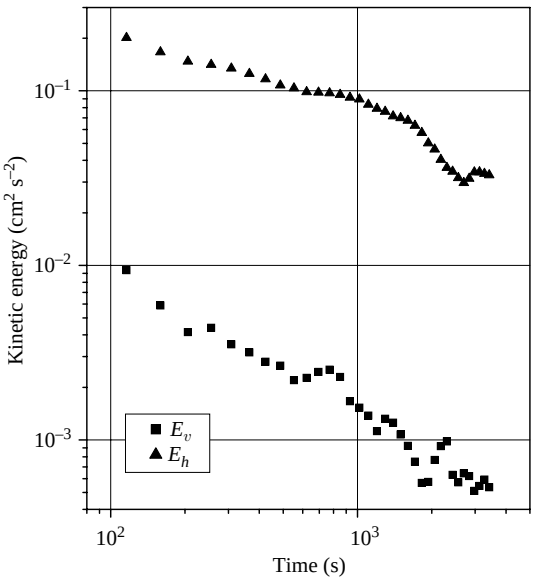

FIGURE 3. Comparison of the horizontal kinetic energy, E_h, and the estimated vertical kinetic energy, E_v. $Re_M = 18\,000$, $Fr_M = 0.34$, $Ro_M = 1.13$.

Such observations can be quantified by measuring the energetic contribution of the vertical velocity, see figure 3. The vertical velocity is evaluated through the continuity equation, that gives, in the Fourier space, for $k_z \neq 0$,

$$\hat{u}_3(\boldsymbol{k}) = -\frac{\boldsymbol{k}_h \cdot \hat{\boldsymbol{u}}_h(\boldsymbol{k})}{k_z}. \tag{3.1}$$

For $k_z = 0$, we choose $\hat{u}_3(k_x, k_z, 0) = 0$, assuming the absence of any mean vertical motion. The comparison of the vertical kinetic energy E_v to the horizontal kinetic energy clearly shows that the contribution of E_v to the total kinetic energy is negligible for the duration of the experiment (less than 5 %) and decreases with time (less than 2 % at the end of the experiment). The energy of the horizontal motion can be therefore considered as the total kinetic energy of the flow within a precision better than 5 %. At the final stage of decay in figure 3, the residual vertical kinetic energy is such that $E_h/E_v \sim 70$.

3.2. *Inhibition of the energy decay by rotation*

The decay of the turbulent kinetic energy $E(t) = \langle u_x^2 + u_y^2 \rangle / 2$, averaged over the measurement volume, is examined in figure 4 for several experiments. The energy and time are normalized by U^2 and M/U respectively. All these experiments correspond to the same initial Reynolds number, equal to 9000, while the Coriolis parameter f and the stratification change. The most obvious effect of rotation is the inhibition of the energy decay: the exponent of the decay power law changes from ~ -1.3 in the non-rotating case to ~ -0.5 for $Ro_M = 0.56$, and for $Ro_M \leqslant 0.2$ there is almost no decay of kinetic energy. This change in energy decay is remarkably not influenced by stratification. For each rotation rate, two different stratifications are compared in figure 4, and no significant dependence on the Froude number is observed. The decay of kinetic energy depends only on the Rossby number.

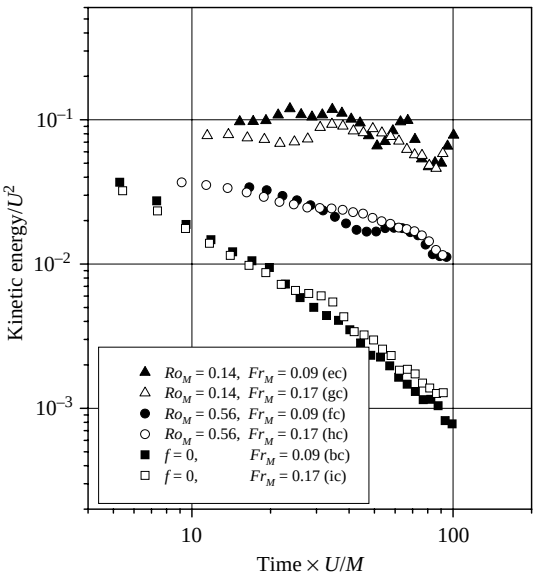

FIGURE 4. Decay of mean kinetic energy for several parameters. The initial Reynolds number is the same for the different experiments, $Re_M = 9000$.

We show later in this paper that the absence of energy decay observed for $Ro_M \leqslant 0.2$ is associated with a k_h^{-3} energy spectrum, the emergence of intense concentrated coherent vortices and a symmetric probability distribution of vertical vorticity. Therefor, the non-dissipative dynamics observed for $Ro_M \leqslant 0.2$, together with the other observations, suggest that, when the rotation rate increases, the turbulence approaches the quasi-geostrophic dynamics, in which a direct energy cascade is absent (like in two-dimensional turbulence).

Notice that fluctuations of the kinetic energy are observed at late times. These occur when large vortices enter or leave the measurement volume. Such fluctuations become more important at late times as the energy is controlled by only a few vortices.

3.3. *Horizontal energy spectra*

The two-dimensional horizontal energy spectrum is calculated as a function of the horizontal wavenumber $k_h = (k_x^2 + k_y^2)^{1/2}$. A two-dimensional fast Fourier transform of the horizontal velocity field is performed in each horizontal plane of the measurement volume. An azimuthal average at radius k_h is taken to obtain the two-dimensional energy spectrum in each plane $E(k_h, z)$. Finally all these horizontal spectra are averaged over the vertical coordinate z to yield the two-dimensional horizontal energy spectrum $E(k_h) = \langle E(k_h, z) \rangle_z$.

These spectra are represented in figure 5 for cases with $Ro_M \leqslant 0.2$. The spectral shape is remarkably constant in time, so the normalized spectra at successive times collapse. Furthermore a k_h^{-3} spectral law is observed. This behaviour, in association with the very small energy dissipation and the cyclones/anticyclones symmetry is consistent with the enstrophy cascade predicted by the quasi-geostrophic theory of Charney. This has also been observed in the numerical simulations of decaying turbulence by Metais *et al.* (1996). Steeper spectra are generally observed in numerical computations of two-dimensional turbulence (McWilliams 1989) and of geostrophic turbulence (McWilliams *et al.* 1999) in association with the emergence of coherent

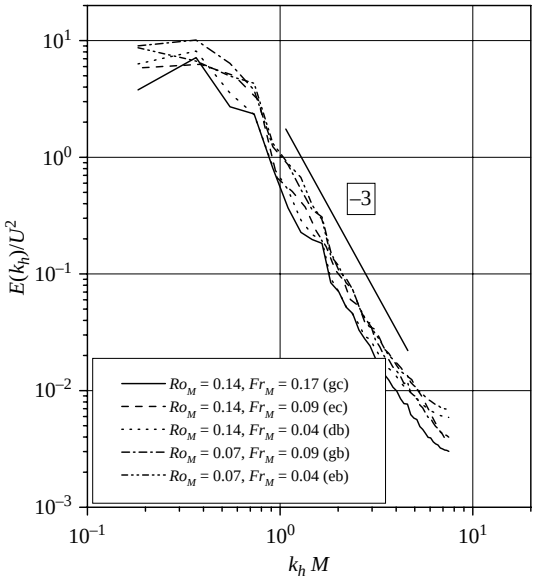

FIGURE 5. Normalized kinetic energy versus normalized horizontal wavenumber at $t \times U/M \sim 15$.

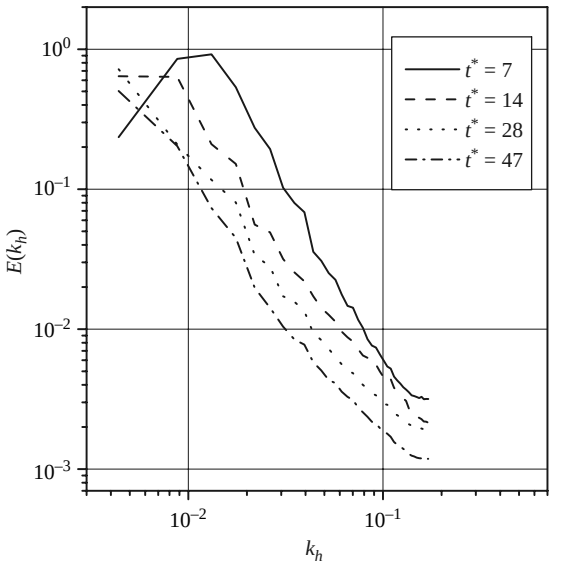

FIGURE 6. Two-dimensional energy spectra at different stages of the experiment in the ageostrophic case. $Re_M = 9000$, $Ro_M = 0.56$, $Fr_M = 0.09$.

vortices. Although the emergence of coherent vortices is also observed in our experiments (see § 5) we did not observe horizontal spectra steeper than k_h^{-3}.

For larger Rossby numbers, for which significant ageostrophic effects are expected, the turbulence spectra do not reach a well-established shape. As illustrated in figure 6, the energy remains confined to the large scales, and the slope at high wavenumbers decreases with time, remaining less steep than -3.

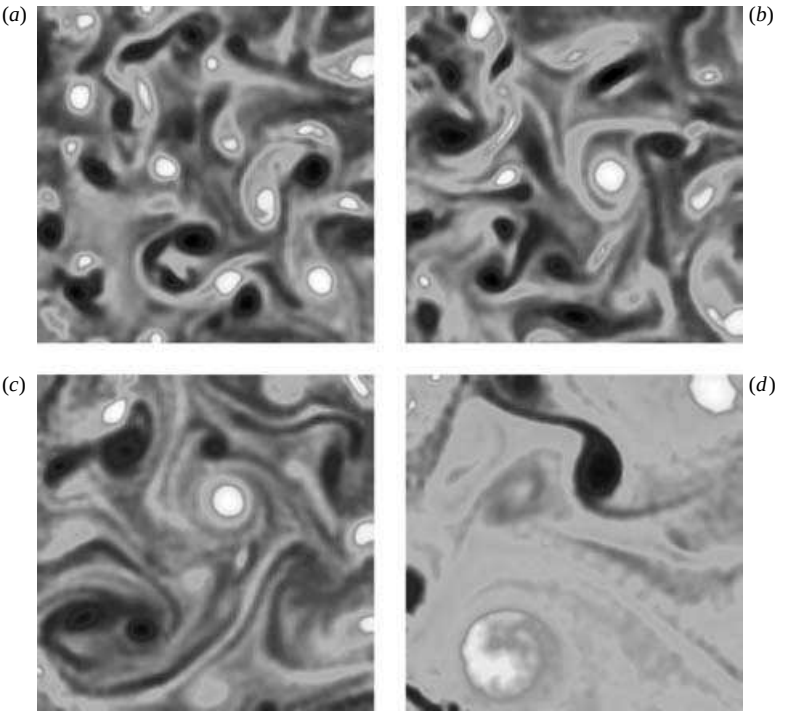

FIGURE 7. Vertical vorticity field in a horizontal plane at four successive times ($t_1 = 377$ s, $t_2 = 619$ s, $t_3 = 915$ s and $t_4 = 3000$ s). The grid was towed from right to left. $Re_M = 4500$, $Fr_M = 0.04$, $Ro_M = 0.07$. The positive values of vertical vorticity are in light grey, negative in dark grey. The size of the represented domain is $250 \times 250\,\mathrm{cm}^2$.

4. General description of the flow

4.1. *Vortex structure and evolution*

Once the regime of horizontal motion is established, long-lived patches of vertical vorticity ω_z, similar to those observed in two-dimensional turbulence, are quickly formed. In figure 7, fields of vertical vorticity are shown at four stages of development during a single experiment.

The vortices interact by mutual advection and undergo merging phenomena; this leads to an increase of their horizontal size. These interactions include multipole formation (dipoles) by pairing of oppositely signed vortices and mergers of like-signed vortices. Properties of the interactions observed in numerical simulations of geostrophic turbulence (see McWilliams 1984, 1989) or rotating turbulence experiments (see Hopfinger *et al.* 1982) are discernible in these experiments. In particular, merging of vortices generally occurs when one of the two vortices is weaker. Vortices with weaker amplitudes are more likely to be destroyed by strain, or absorbed by merging. When two close together vortices have approximately the same strength, the interaction eventually leads to the merging of the two and a symmetrization of the resulting vortex. More generally, the interactions produce shearing deformation. Strong distortion occurs, including the production of elongated horizontal filaments of vertical vorticity which leads to a reduction in the vertical enstrophy.

As time goes on, the number of intense vortices decreases, they become sparser and the encounters occur less frequently but their horizontal size keeps growing. The final

stage of evolution is well represented by figure 7(*d*). The flow consists of a few robust vortices, surrounded by weak vertical vorticity characterized by elongated filaments at small scales. The turbulent field becomes progressively more inhomogeneous and vortices with increasing size are separated by large unstructured areas. For very late times, the size of the structures is limited by the width of the channel, and the horizontal growth is stopped.

For moderate rotation rates ($Ro_M \geqslant 0.2$), cyclonic vortices are found to be more abundant and stronger than anticyclonic vortices. Moreover, cyclonic vortices exhibit greater axisymmetry and are more robust in the presence of ambient strain. While a horizontal symmetrization process is observed after merging for the cyclonic vortices, the anticyclonic vortices remain elongated in the horizontal plane. This tendency toward cyclonic predominance will be discussed in § 5. By contrast, cyclones and anticyclones have the same properties in the quasi-geostrophic model, as a mathematical symmetry. This symmetry is for instance observed in the numerical simulations (see McWilliams 1989).

In the absence of rotation, cyclones and anticyclones are obviously found in equal numbers and strengths. They are more diffusive and less sparse than when rotation is present. Expulsion of vorticity filaments also seems to be reduced.

4.2. *Antagonistic effect of rotation and stratification and three-dimensional structure of the flow*

The competition between stratification and rotation is illustrated in figures 8 and 9: horizontal layering is obtained when stratification dominates, while columnar structures are obtained when rotation dominates. These figures show successive three-dimensional views of the vertical vorticity fields represented by iso-surfaces, for two different rotation rates. In both cases, the initial wake of the rake is made of coherent columnar vortices, extending through the whole fluid depth of the layer.

In the absence of rotation, an instability mechanism for stratified columnar vortices, called the zig-zag instability, was proposed by Billant *et al.* (2000) and Billant & Chomaz (2000) to explain the layering. The vertical scale selected by this mechanism is proportional to U/N. However, Praud *et al.* (2005) showed that the vertical scale in the turbulent regime is not influenced by this initial instability mechanism and exhibits no dependence on the stratification. Moreover, as we will show in § 4.3, under the joint effects of rotation and stratification, the aspect ratio of these 'pancake' vortices is prescribed by the ratio f/N.

For moderate rotation rates, as in the case presented in figure 8 ($Ro_M = 0.28$, $f/N = 0.15$), the stabilizing effect of rotation is not sufficiently strong to resist the straining deformation induced by the other vortices and vertical fragmentation occurs. The shed vortices rapidly become unstable and lose their vertical coherence under the action of the mutual advection induced by the neighbouring vorticity distribution, producing multiple layers of eddies. The flow then consists of patches of vertical vorticity localized in space, which look similar to the so-called 'pancake' vortices observed by Fincham *et al.* (1996) or Praud *et al.* (2005) in purely stratified turbulence experiments.

The destabilization of the columnar vortices that occurs for low values of f/N, is consistent with the results of Dritschel & de la Torre Juarez (1996) and Dritschel, de la Torre Juarez & Ambaum (1999). Numerically investigating the stability of columnar vortices in quasi geostrophic flows, they observed that two-dimensional vortices of diameter L smaller than the Rossby deformation radius, $L_R = HN/f$ (H is the vertical height of the column), are unstable to three-dimensional disturbances and

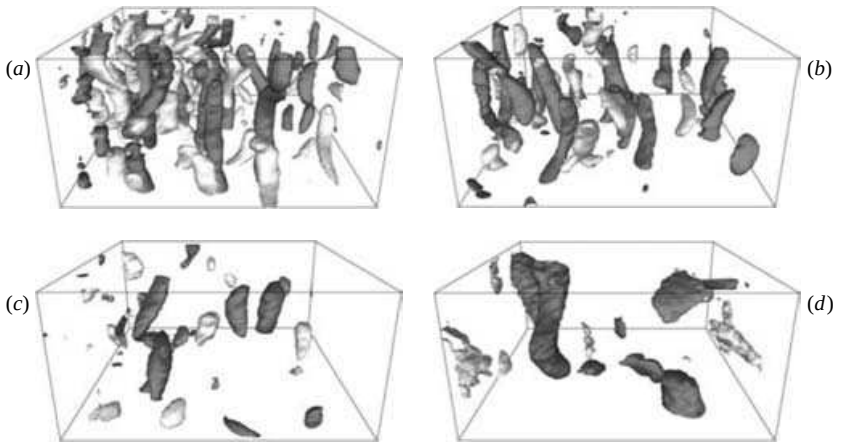

FIGURE 8. Evolution of the three-dimensional structure of the vertical vorticity component represented by iso-surfaces at $t = 280$ s, $t = 600$ s, $t = 1100$ s and $t = 2000$ s for $f/N = 0.15$. The vorticity value is 35 % of the maximum of $|\omega_z|$. The positive values of ω_z are in dark grey while the negative values are in light grey. The rake is towed from right to left. $Re_M = 4500$, $Ro_M = 0.28$, $Fr_M = 0.04$. The size of the represented volume is $250 \times 250 \times 45\,\mathrm{cm}^3$ and the vertical axis is stretched three times to enhance the visualization.

break down. Dritschel & de la Torre Juarez (1996) found instability for $L < L_R/3$ and Dritschel *et al.* (1999) for $L < L_R/2$. In the present experiments, the initial height is the depth of the fluid ($H = 90$ cm). We observe a rapid fragmentation of the columnar vortices produced in the wake of the rake for $f/N \leqslant 0.6$. This transition corresponds to $L_R = 1.45$. The vortex size, of the order of the grid mesh 45 cm, is close to $L_R/3$, in rough agreement with the stability results.

Fragmentation is generally followed by new attachments of like-sign vortices whose cores are separated vertically. Thus, as the processes of attachment and fragmentation continuously act, the vertical extent is highly variable in both space and time. The dominance of the cyclonic vortices is clearly observed in this process: they tend to be vertically coherent, whereas the anticyclones remain fragmented with a smaller vertical scale.

By contrast, for high rotation rates ($Ro_M = 0.07$, $f/N = 1.2$), the wake remains quasi-two-dimensional (figure 9), with vortices strongly correlated along the vertical. These columnar vortices are very robust, as they do not lose their vertical coherence during strong interactions and close encounters. This development of vortical columns is more pronounced as f/N is increased. A progressive transition from the 'pancake' eddies of purely stratified turbulence to such regimes with vertical columns is observed as the rotation rate is increased.

4.3. *Length-scale evolution*

4.3.1. *Horizontal length scales*

The increase of the horizontal size of the vortices observed in figures 8 and 9 can be characterized in terms of the horizontal integral scale L_h. This scale is obtained as the integral of the longitudinal autocorrelation function of the horizontal velocity, taken up to its first zero crossing. The growth of L_h for various experiments is represented in figure 10. A good collapse of all the curves is observed over a large range of Rossby and Froude numbers: the growth of L_h is remarkably independent of rotation and

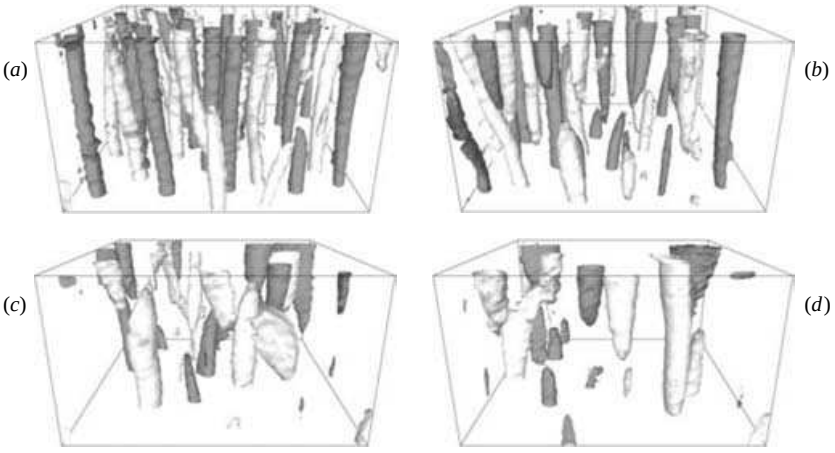

FIGURE 9. As figure 8 but for $f/N = 1.2$, $Ro_M = 0.07$, $Fr_M = 0.09$.

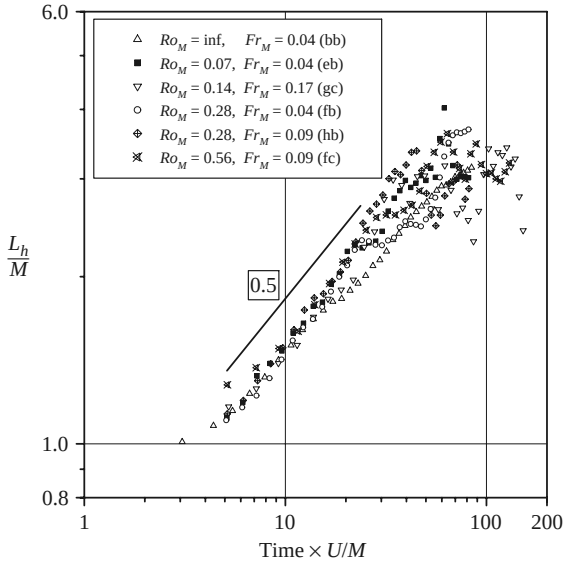

FIGURE 10. Evolution of the horizontal integral scale, L_h for various experiments.

stratification. It approximately follows a power law

$$L_h/M \simeq 0.5t^{*0.5}, \tag{4.1}$$

where t^* is the non-dimensional horizontal advective time: $t^* = tU/M$. The value of the exponent is close to what is obtained in decaying three-dimensional homogeneous turbulence, as well as in purely two-dimensional turbulence (see Bracco *et al.* 2000). Such similar behaviour of L_h for very different dynamical regimes is remarkable.

For late times, the growth becomes slower and the plot becomes scattered. Indeed, the number of vortices present in the measurement area decreases with time and the correlation function fluctuates strongly depending on the relative position of these vortices: when $L_h \sim 100$ cm, there are less than four vortices in the field of view. Moreover the growth of L_h starts to be limited by the width of the channel.

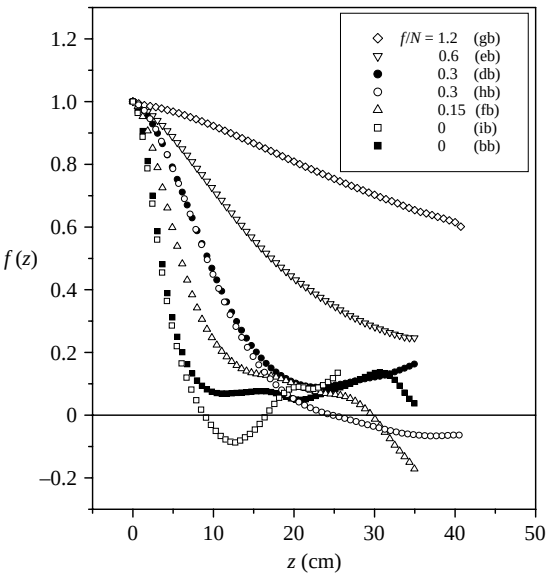

FIGURE 11. The transverse velocity correlation function $f(z)$, for various experiments at $t \times U/M \sim 11$, $Re_M = 4500$.

4.3.2. *Vertical length scales*

Since the horizontal velocity component dominates the flow, we estimate the vertical integral scale from the transverse autocorrelation function of the horizontal velocity. However, for a number of experiments, this function remains positive for all accessible vertical separations z, implying that the vertical integral scale is greater than the vertical extent of the measurement volume. The vertical scale is thus examined directly from the correlation function, as shown in figure 11. The competing effects of stratification and rotation on the vertical correlation is clearly visible, confirming the qualitative discussion of § 4.2: the vertical correlation clearly increases with the ratio f/N. Note however, that even when rotation is dominant over stratification (case $f/N = 1.2$), the correlation function still significantly decreases with z, that is, the flow is not purely two-dimensional and the columns are tilted as seen in figure 9.

The vertical scale depends only on the ratio f/N. This is suggested by comparing the two curves with $f/N = 0.3$. This is also observed in the purely stratified case ($f/N = 0$) where stratification does not influence the integral vertical scale (Praud *et al.* 2005). In the previous subsection, it was also shown that the horizontal scale does not depend on stratification, so the aspect ratio between vertical and horizontal integral scales depends only on f/N. This result, consistent with the quasi-geostrophic model, seems to apply in all the regimes of stratified rotating turbulence.

When the vertical integral scale can be measured (for $f/N \leqslant 0.3$), it often fluctuates, as can be seen in figure 12(a). The attachment of like-sign vortices at different altitudes results in a sudden increase of the integral vertical scale. By contrast, vortex fragmentation by the strain field induced by neighbouring vortices results in a sudden loss of vertical coherence and a decrease of the vertical correlation length. Nevertheless, in all the experiments a global increase of the integral vertical scale with time is observed. This tendency is partially due to viscous diffusion but mainly to the fact that attachment events are more common than fragmentation events, as already noticed in numerical simulations (see McWilliams 1989).

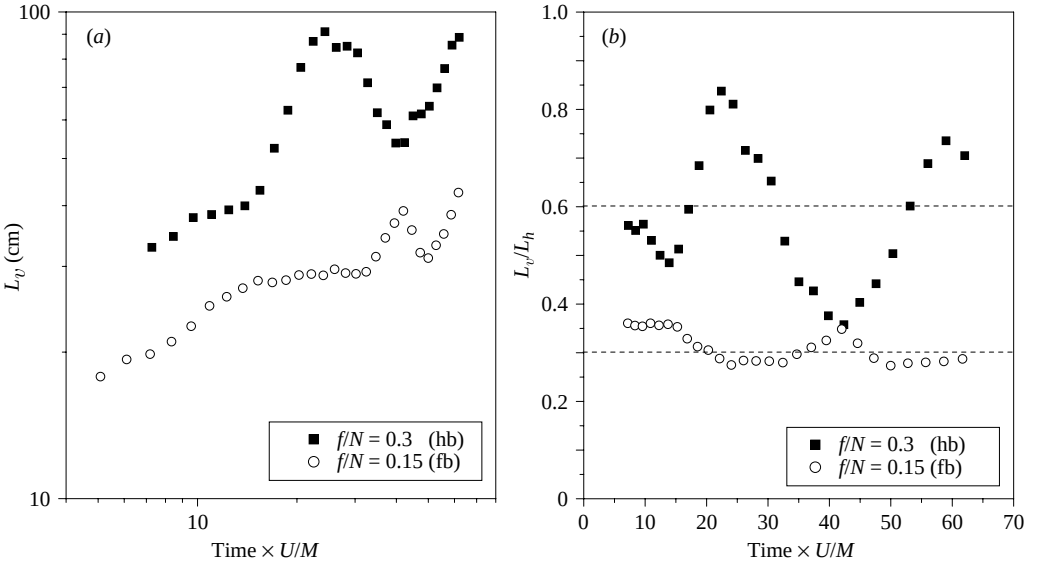

FIGURE 12. Evolution of (a) the vertical integral scale L_v and (b) the aspect ratio of the structure. $Re_M = 4500$.

In the horizontal directions, the merger events and the destruction of the weaker vortices always lead to an increase of L_h, while the vertical integral scale can either grow or shrink. However, as can be seen in figure 12(b), for $f \neq 0$, the ratio L_v/L_h oscillates around a constant value, which is proportional to f/N. The results show that for the joint conditions of rotation and stratification, these eddies take the form of lens-like vortices with aspect ratio $L_v/L_h \sim 2f/N$. Such a proportionality characterizes the geostrophic regime.

The proportionality of the aspect ratio to f/N and its time independence agree well with the results of McWilliams *et al.* (1999). From numerical simulation of decaying geostrophic turbulence, he found that $\langle h/r \rangle \sim 0.83 f/N$ and is globally conserved with time (he defined h and r respectively as the half-height and the radius of a vortex element). These data lead to an average height-to-width aspect ratio of vortices of $1.7 f/N$ which is comparable to the $2f/N$ found in the present study.

In the purely stratified regime, the flow degenerates into an assembly of quasi-two-dimensional flows in layers. An important role is then played by viscosity (see Praud *et al.* 2005) which limits the vertical shear and the vertical scale grows according to a diffusive process, $L_v \simeq 2(\nu t)^{0.5}$. A definite change in the nature of the dynamics occurs under the influence of rotation: the vertical scale is no longer controlled by viscosity; this is discussed in the next section.

4.4. *Vanishing effect of the vertical gradients*

A direct consequence of the increase of the vertical scale with f/N is the reduction of the vertical gradients and therefore the reduction of their contribution to the total enstrophy and to the viscous energy dissipation. This effect is illustrated well in figure 13, which shows the evolution of the contributions of $\langle \omega_z^2 \rangle$ and $\langle \omega_h^2 \rangle$ for different values of f/N, at a given initial Reynolds number ($Re_M = 9000$). The scatter observed in the estimation of $\langle \omega_h^2 \rangle$ for the case $f/N = 1.2$ is due to measurement noise (as the vertical gradient is weak in this case and more difficult to distinguish from noise). Nevertheless, figure 13 clearly shows that the relative contribution of

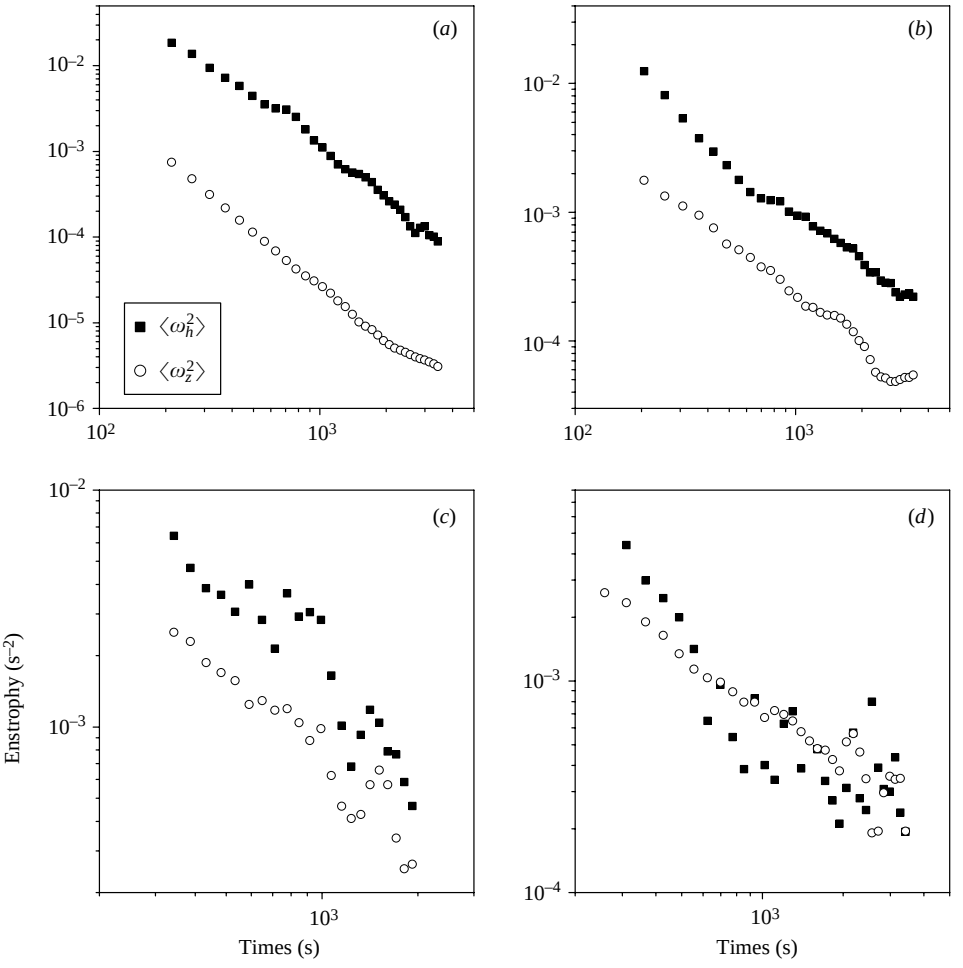

FIGURE 13. Vertical vorticity, $\langle\omega_z^2\rangle$, and horizontal vorticity $\langle\omega_h^2\rangle$ decay for increasing values of f/N. $Re_M = 9000$. (*a*) $f/N = 0$, (*b*) $f/N = 0.3$, (*c*) $f/N = 0.6$, (*d*) $f/N = 1.2$.

the vertical gradients decreases with increasing f/N. For $f/N = 0$ the enstrophy is entirely dominated by the horizontal vorticity (then equivalent to the vertical shear) which confirms the layered structure of the flow and is consistent with numerical simulations (see Herring & Metais 1989; Smith & Waleffe 2002) and experiments on stratified turbulence (see Fincham *et al.* 1996; Praud *et al.* 2005). The organization of the flow into thin 'pancake' eddies localized in space and bounded by horizontal vortex sheets leads to strong vertical shear. With increasing f/N, the contribution of the horizontal vorticity progressively decreases and becomes of the same order as the vertical vorticity when $f/N = 1.2$.

The ratio $\alpha = (\langle\omega_z^2\rangle/\langle\omega_h^2\rangle)^{1/2}$ can also be considered as the aspect ratio of the eddies based on the vertical to the horizontal Taylor microscales, defined as

$$\lambda_h = \left[\frac{0.5\langle u_x^2 + u_y^2\rangle}{\langle w_z^2\rangle}\right]^{1/2}, \quad \lambda_v = \left[\frac{\langle u_x^2 + u_y^2\rangle}{\langle \omega_x^2 + \omega_y^2\rangle}\right]^{1/2}. \tag{4.2}$$

As for the aspect ratio based on the integral scale, α is approximately conserved with time in the presence of rotation: the decay of $\langle\omega_h^2\rangle$ and $\langle\omega_z^2\rangle$ follows approximately

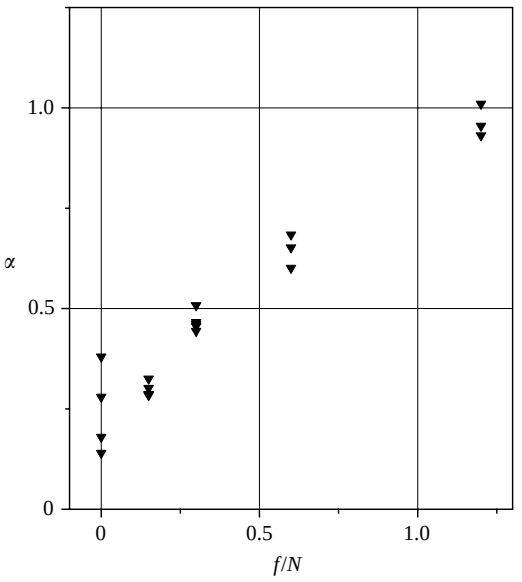

FIGURE 14. Ratio $\alpha = (\langle \omega_z^2 \rangle / \langle \omega_h^2 \rangle)^{1/2}$ versus f/N, averaged over the time interval [200...3000 s]. Experiments with different Re_M are used for each value of f/N.

the same law and their relative contribution to the total enstrophy remains the same for the duration of the experiment.

The time-averaged value of α is plotted versus f/N in figure 14. This ratio is a monotonically increasing function of f/N, in agreement with other scale estimates. Note that α is not quite a linear function of f/N; this indicates some departure from the quasi-geostrophic model.

Remarkably, for $f \neq 0$ (N fixed), α does not depend significantly on the Reynolds number. This is consistent with the fact that energy dissipation (mainly the product of the shear squared and viscosity) tends to zero in the limit of small viscosity. This contrasts with the purely stratified case ($f = 0$, also represented in figure 14) for which α definitely decreases with increasing Re: here $\alpha \sim Re^{-0.5}$ as described by Praud *et al.* (2005) so that the energy dissipation ($\sim Re\,\alpha^2$) is independent of viscosity. The transition between these two regimes cannot be seen in figure 14. Further experiments at low rotation rates would be needed to analyse this transition.

5. Intermittency and asymmetry of the vorticity distribution

We have discussed the natural tendency of rotating stratified turbulence to form coherent vortices that can be identified and tracked for periods of time that are long compared with their typical turnover times. Figure 7 provides an example. When rotation is present, most observed vortices are monopoles but dipoles or tripoles can be temporarily formed. As time goes on, the number of structures decreases, and those remaining tend to dominate over the background vorticity.

An objective statistical measure of vortex dominance and therefore of the intermittent character of the flow is the flatness,

$$Ku = \frac{\langle \omega^4 \rangle}{\langle \omega^2 \rangle^2} \tag{5.1}$$

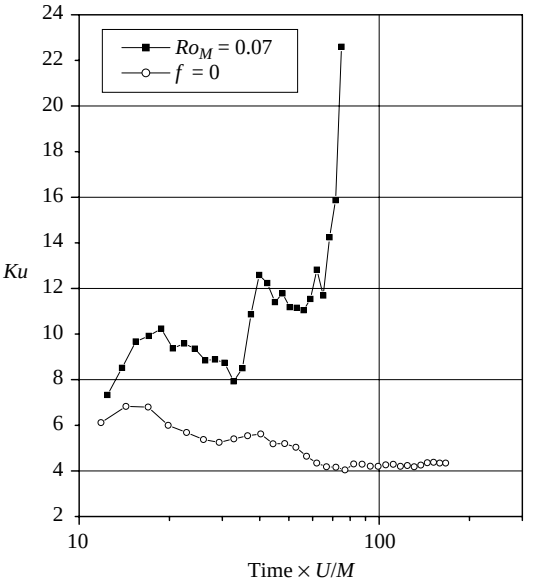

FIGURE 15. $Ku(t) = \langle\omega^4\rangle/\langle\omega^2\rangle^2$ for $Ro_M = 0.07$ (gb) and $f = 0$ (bc).

which can be interpreted as the inverse of the area fraction occupied by the vortices. Its evolution is represented in figure 15 for $f = 0$ and for $Ro_M = 0.07$. In all the experiments, an initial value of Ku close to 7 is obtained. This relatively large value is due to vortex shedding behind the rake creating compact coherent vortices. In the absence of rotation, Ku decreases to reach a value close to 3, the characteristic value for a Gaussian field. When rotation is present, Ku increases from a starting value of 7, and can reach values greater than 20. The large values of the flatness characterize a highly intermittent field, in which the vorticity is concentrated and occupies a relatively small volume of the turbulent field.

The intermittent character of the flow and the cyclone/anticyclone asymmetry can be best seen from the probability distributions of the vertical vorticity for several different initial Rossby numbers (figure 16). For $Ro_M \leqslant 0.2$ we observe a strong intermittency with no asymmetry, similar to that obtained with a quasi-geostrophic model. Cyclones and anticyclones are found in equal strengths and proportions: the vorticity distributions have big, almost symmetric tails, corresponding to a relatively large probability of occurrence for values much larger than the root mean square vorticity. It is important to notice that this behaviour is associated with the absence of significant energy dissipation (see § 3.2). All these properties are in agreement with quasi-geostrophic dynamics, as discussed for instance by McWilliams (1990) and McWilliams *et al.* (1999).

For larger Rossby numbers ($Ro_M \geqslant 0.2$) a clear dominance of cyclonic vorticity is observed. The regions of strong cyclonic vorticity are highly concentrated, corresponding to the positive tails in the probability distribution. By contrast, the anticyclonic part of the vorticity distribution drops steeply. This result is consistent with the qualitative observations of columnar cyclonic vortices amidst deformed, non-axisymmetric and fragmented anticyclonic vortices. This asymmetry is inconsistent with the quasi-geostrophic model, but is predicted by models including some higher-order corrections. The bias for cyclones is for instance predicted by a surface geostrophic model (Hakim

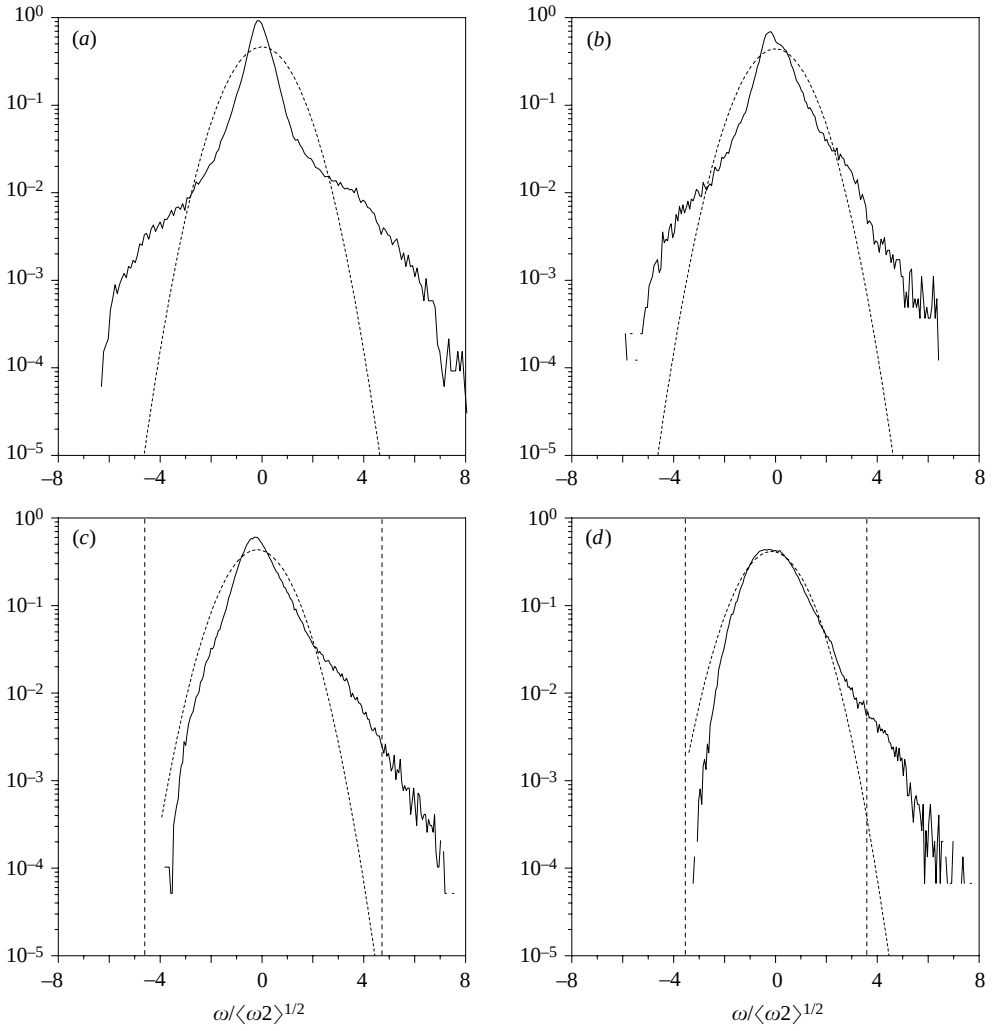

FIGURE 16. Normalized probability distribution of vertical vorticity for several values of f/N at $t \times U/M = 50$. Gaussian distributions with equivalent variances are plotted in dotted lines. In the four cases, the Froude Fr_M is equal to 0.09, and only the rotation is changed: (*a*) $Ro_M = 0.07$ (gb), (*b*) $Ro_M = 0.14$ (ec), (*c*) $Ro_M = 0.28$ (hb), (*d*) $Ro_M = 0.56$ (fc). The value of the normalized Coriolis parameter $f/\langle w_z^2\rangle^{1/2}$, corresponding to $Ro = 1$, is represented by a vertical dashed line. For the two higher rotation rates (*a*, *b*), this value is outside the plotting range and is not represented: (*a*) $f/\langle w_z^2\rangle^{1/2} = 13$ and for (*b*) $f/\langle w_z^2\rangle^{1/2} = 8.57$.

et al. 2002) (Muraki, Snyder & Rotunno 1999). In numerical simulations of this model, for moderate Rossby number $Ro \sim O(0.1)$, Hakim *et al.* (2002) indeed observed a distinct dynamical asymmetry favouring strong compact cyclones and weak broad anticyclones.

A local Rossby number, $Ro_{local} = (\omega_z^2)^{1/2}/f$, can be associated with any region in these probability distributions. It can be seen in figure 16, that for the asymmetric cases corresponding to Rossby numbers of order 1, the local Rossby number exceeds unity in the cyclonic vortex cores but seems to 'saturate' at values close to unity for the anticyclonic regions. Here the absolute vorticity $-f + \omega_z$ is zero and locally there is no effective rotation, a condition that is not favourable to vortex persistence.

We recover here results from linear stability of rotating flows which predict unstable strong anticyclones ($Ro_{local} > 1$) and possibly stable weak anticyclones ($Ro_{local} \leqslant 1$). This destabilization of strong anticyclones for $Ro \sim O(1)$ is indeed consistent with the centrifugal stability arguments that yield a stability/instability crossover for anticyclones when $\omega_z(r) = -f$ (Kloosterziel & van Heijst 1991; Pedley 1969). Instability criteria were also found in the more general or complex flows by Cambon *et al.* (1994) and Leblanc & Cambon (1997, 1998) but all these stability studies lead to the conclusion that strong anticyclonic vortices are unstable while weak anticyclones and cyclones are stable. Our results are consistent with this conclusion.

The predominance of cyclonic vorticity for moderate rotation rates ($Ro \sim O(1)$) was previously observed in purely rotating turbulence, either in numerical simulation (Bartello *et al.* 1994; Smith & Waleffe 1999; Godeferd & Lollini 1999) or in experiments (Hopfinger *et al.* 1982). A similar emergence of coherent vortices, with dominance of cyclones at moderate Rossby numbers, has been also obtained by Longhetto *et al.* (2002) with the same device as for the non-stratified case. Moreover, like Hopfinger *et al.* (1982) they observed that when the Rossby number gets smaller, the symmetry is restored. Note that strong anticyclones, with $\omega_z < -f$, can be produced just behind the rake as Kármán vortex streets, but they do not persist in the established turbulence.

In the stratified case with no rotation, there is no reason for the flow to exhibit any cyclonic/anticyclonic asymmetry; this is confirmed by the measurements. Furthermore, the probability distribution function then exhibits a quasi-Gaussian behaviour, which marks the absence of intense vortices. This demonstrates one of the profound differences between the stratified and stratified rotating cases.

6. Conclusion

The influence of rotation and stratification on decaying grid turbulence has been studied with our experimental system. We have covered the parameter space from the homogeneous to the strongly stratified case ($Fr \sim 10^{-2}$) and obtained strong rotation effects ($Ro \sim 10^{-2}$), while the Reynolds number was kept sufficiently large (about 10^4) to approach the inertial regime. This is confirmed by the invariance of the results with respect to changes in the Reynolds number. The scanning correlation imaging velocimetry technique provides time-resolved velocity fields in a volume, with direct access to scales at which energy is dissipated by viscosity.

An important effect of rotation is the inhibition of the energy decay as illustrated in figure 4. As rotation increases the dynamics undergoes a transition from a highly dissipative regime ($f = 0$, $N \neq 0$) to a non-dissipative regime at low Rossby number. We find that for $Ro_M \leqslant 0.2$ $Ro \leqslant 0.02$ based on the velocity r.m.s. and the integral scale), the energy decay becomes negligible. However, the dissipation is influenced by Ekman layers. This is the dominant source of dissipation in the unstratified rotating case, as found for instance by Longhetto *et al.* (2002) during experiments with the same device as we used. We find that this effect also controls dissipation for the final decay in the stratified cases with the strongest rotation, when the vertical integral scale corresponds to the depth of the tank. However, the combined effects of stratification and rotation cause the dissipation to be significantly lower than in the non-stratified case, due to the confinement of the Ekman layer pumping.

This non-dissipative regime is also associated with a k_h^{-3} energy spectrum and a symmetric probability distribution of vertical vorticity which involves tails corresponding to the emergence of intense vortices. These features are consistent with

the quasi-geostrophic model of Charney (1971) which predicts, in the limit of small Rossby and Froude numbers, the absence of a direct energy cascade and a direct cascade of enstrophy, as in two dimensional turbulence. Some of the properties observed in this regime can alternatively be described in terms of wave theories. For instance, Cambon *et al.* (2004) obtained the emergence of k_h^{-3} energy spectrum in purely rotating turbulence by the nonlinear interactions of dispersive waves. However, the emergence of intense vortices and the high values of the kurtosis (figures 7 and 15) are typical of quasi-geostrophic dynamics and are not consistent with quasi-Gaussian wave theories. These observations tend to confirm that, in this regime, the effect of inertial–gravity waves remains negligible and that the spectrum is associated with the enstrophy cascade.

These experiments provide the possibility of investigating the breakdown of this non-dissipative quasi-geostrophic regime, as the Rossby number is increased. The first ageostrophic effect is the systematic suppression of the intense anticyclonic vortices with local Rossby number $\langle w_z^2 \rangle^{1/2}/f$ larger than unity, as shown in figure 16. The absolute vorticity in such vortex cores vanishes. We find that anticyclonic vortices with higher local Rossby numbers, such as those produced directly in the wake of the rake, are quickly destroyed.

Even for the weakest rotation (largest Rossby number) used in our experiments the vertical shear (or horizontal vorticity) is controlled by the geostrophic balance: it is found to be in a ratio f/N with the horizontal shear and is independent of viscosity (see figure 14). By contrast, in isotropic homogeneous turbulence, and in non-rotating stratified turbulence, the vertical shear is related to the Taylor microscale and is controlled by viscous dissipative effects.

In this transitional regime between the non-dissipative regime ($Ro \leqslant 0.02$) and the non-rotating stratified turbulence, we observe that energy dissipation depends only on rotation, with no dependence on stratification, as shown in figure 4. By contrast the vertical shear is still controlled by the geostrophic balance and therefore depends on stratification (it scales with f/N alone). Therefore the dissipation cannot be approximated from the vertical shear ($\nu\omega_h^2$) as in the non-rotating stratified case and other components have to be taken into account. In this transitional regime, unlike in the non-dissipative regime ($Ro \to 0$, $Fr \to 0$), we cannot exclude significant wave effects and wave theories could be relevant to interpret some of the results observed.

In this regime, the decrease of the energy dissipation with increasing rotation rate and its independence from the stratification may indicate that the mechanisms of energy transfer are close to the ones observed in purely rotating turbulence (Waleffe 1993; Cambon *et al.* 1997). Energy dissipation is necessarily controlled by nonlinear energy transfers between modes. Nevertheless, some aspects of the dynamics may be accounted for well by linear theories, as proposed by Hanazaki (2002) for rotating stratified turbulence. Using the rapid distortion theory (RDT) he has shown that the integrated quantities depend only on f/N, a result in agreement with our findings on the vertical scale. The high anisotropy ratio between horizontal and vertical kinetic energy seems also to be consistent with the RDT for initially horizontal turbulence. Indeed, equations (5.09)–(5.11) of Hanazaki (2002) give, for the long-time asymptotics and for $f/N = 0.3$, a ratio $E_h/E_v \sim 75$ close to our estimate $E_h/E_v \sim 70$, for the final stage of the decay in figure 3. This large ratio is the consequence of the particular initial conditions with purely horizontal velocity (zero 'wave energy'). This corresponds to our experimental forcing by a rake of vertical plates. We expect that this initial condition would be forgotten through a phase of three-dimensional turbulence, but this agreement with the RDT theory may indicate that the system keeps track of

the initial conditions. This point should be investigated by comparison with forcing by a grid instead of a rake of vertical plates and by direct measurement of energy transfers.

Further work would be required to study the transition between the energy-conserving dynamics and the dissipative dynamics of non-rotating stratified turbulence, with a more detailed analysis of non-geostrophic effects like front formation and wave–vortex interactions.

The authors would like to thank Claude Cambon and the referees for their constructive comments on the manuscript. The author also thank the support of Henri Didelle and René Carcel for the design and realization of the set-up. The work presented here has been supported by the European Commission project HYDRIV under contract HPRI-1999-50019 of the FP5 Improving Human Potential programme)

REFERENCES

Babin, A., Mahalov, A. & Nicolaenco, B. 1998 On nonlinear baroclinics waves and adjustment of pancake dynamics. *Theoret. Comput. Fluid Dyn.* **11**, 215–235.

Bardina, J., Ferziger, J. M. & Rogallo, R. S. 1985 Effect of rotation on isotropic turbulence: computation and modelling. *J. Fluid Mech.* **154**, 321–336.

Bartello, P. 1995 Geostrophic adjustment and inverse cascades in rotating stratified turbulence. *J. Atmos. Sci.* **52**, 4410–4428.

Bartello, P., Metais, O. & Lesieur, M. 1994 Coherent structures in rotating three-dimensional turbulence. *J. Fluid Mech.* **273**, 1–29.

Billant, P. & Chomaz, J. M. 2000 Theoretical analysis of the zigzag instability of a vertical columnar vortex pair in a strongly stratified fluid. *J. Fluid Mech.* **419**, 22–63.

Billant, P., Chomaz, J. M. & Huerre, P. 2000 Experimental evidence for a new instability of a vertical columnar vortex pair in a strongly stratified fluid. *J. Fluid Mech.* **418**, 167–188.

Bracco, A., McWilliams, J. C., Murantes, G., Provenzale, A. & Weiss, J. B. 2000 Revisiting freely, decaying two-dimensional turbulence at millenium resolution. *Phys. Fluids* **12**, 2931–2942.

Cambon, C. 2001 Turbulence and vortex structures in rotating and stratified flows. *Eur. J. Mech.* B **20**, 489–510.

Cambon, C., Benoît, J. P., Shao, L. & Jaquin, L. 1994 Stability analysis and large eddy simulation of rotating turbulence with organized eddies. *J. Fluid Mech.* **278**, 175–200.

Cambon, C., Mansour, N. N. & Godeferd, F. S. 1997 Energy transfer in rotation turbulence. *J. Fluid Mech.* **337**, 303–332.

Cambon, C., Rubinstein, R. & Godeferd, F. S. 2004 Advanced in wave turbulence: rapidely rotating flows. *New J. Physics* **6** (73), 1–29.

Charney, J. G. 1971 Geostrophic turbulence. *J. Atmos. Sci.* **28**, 1087–1095.

Dritschel, D. G. & de la Torre Juarez, M. 1996 The instability and breakdown of tall columnar vortices in a quasi-geostrophic fluid. *J. Fluid Mech.* **328**, 129–160.

Dritschel, D. G., de la Torre Juarez, M. & Ambaum, M. H. P. 1999 The three dimensional vortical nature of atmospheric and oceanic turbulent flows. *Phys. Fluids* **11**, 1512–1520.

Fincham, A. M. 1998 3D measurement of vortex structures in stratified fluid flows. In *IUTAM Symp., Simulation and Identification of Organized Structures in Flows* (ed. E. J. H. J. N. Soerensen & N. Aubry), pp. 273–287.

Fincham, A. M., Maxworthy, T. & Spedding, G. R. 1996 Energy dissipation and vortex structure in freely decaying stratified grid turbulence. *Dyn. Atmos. Oceans* **23**, 155–169.

Fincham, A. M. & Spedding, G. R. 1997 Low cost, high resolution DPIV for measurement of turbulent fluid flow. *Exps. Fluids* **23**, 449–462.

Godeferd, F. S. & Lollini, L. 1999 Direct numerical simulatins of turbulence with confinement and rotation. *J. Fluid Mech.* **393**, 257–308.

Godeferd, F. S. & Staquet, C. 2003 Statistical modelling and direct numerical simulations of decaying stably stratified turbulence. part 2. large-scale and small-scale anisotropy. *J. Fluid Mech.* **486**, 115–159.

Hakim, G. J., Snyder, C. & Muraki, D. J. 2002 A new surface model for cyclone-antcyclone asymetry. *J. Atmos. Sci.* **59**, 2405–2420.

Hanazaki, H. 2002 Linear process in stably and unstably stratified rotating turbulence. *J. Fluid Mech.* **465**, 157–190.

Herring, J. 1980 Statistical theory of quasi-geostrophic turbulence. *J. Atmos. Sci.* **37**, 969–977.

Herring, J. R. & Metais, O. 1989 Numerical simulation in forced stably stratified turbulence. *J. Fluid Mech.* **202**, 97–115.

Hopfinger, E. J., Browand, F. K. & Gagne, Y. 1982 Turbulence and waves in a rotating tank. *J. Fluid Mech.* **25**, 505–534.

Kloosterziel, R. & van Heijst, G. J. F. 1991 An experimental study of unstable barotropic vortices in a rotating fluid. *J. Fluid Mech.* **223**, 1–24.

Leblanc, S. & Cambon, C. 1997 On the three dimensional instabilities of plane flows subjected to coriolis force. *Phys. Fluids* **9**, 1307–1316.

Leblanc, S. & Cambon, C. 1998 Effects of the coriolis force on the stability of stuart vortices. *J. Fluid Mech.* **356**, 353–379.

Lilly, D. K. 1983 Stratified turbulence and the meso-scale variability of the atmosphere. *J. Atmos. Sci.* **40**, 749–761.

Linden, P. F., Boubnov, B. M. & Dalziel, S. B. 1985 Source-sink turbulence in a rotating stratified fluid. *J. Fluid Mech.* **298**, 81–112.

Longhetto, A., Montabone, L., Provenzale, A., Didelle, H. & Giraud, C. 2002 Coherent vortices in rotating flows: a laboratory view. *Il Nuovo Cimento* **25**, 233–249.

McWilliams, J. C. 1984 The emergence of isolated vortices in turbulent flow. *J. Fluid Mech.* **146**, 21–43.

McWilliams, J. C. 1989 Statistical properties of decaying geostrophic turbulence. *J. Fluid Mech.* **198**, 199–230.

McWilliams, J. C. 1990 The vortices of geostrophic turbulence. *J. Fluid Mech.* **219**, 387–404.

McWilliams, J. C., Weiss, J. B. & Yavneh, I. 1999 The vortices of homogeneous geostrophic turbulence. *J. Fluid Mech.* **401**, 1–26.

Metais, O., Bartello, P., Garnier, E., Riley, J. J. & Lesieur, M. 1996 Inverse cascade in stably stratified rotating turbulence. *Dyn. Atmos. Oceans* **23**, 193–203.

Muraki, D. J., Snyder, C. & Rotunno, R. 1999 The next order corrections to quasigeostrophic theory. *J. Atmos. Sci.* **56**, 1547–1560.

Pedley, T. J. 1969 On the stability of viscous flow in a rapidly rotating pipe. *J. Fluid Mech.* **35**, 97–115.

Praud, O. & Fincham, A. 2005 The structure and dynamics of dipolar vortices in a stratified fluid. *J. Fluid Mech.* **544**, 1–22.

Praud, O., Fincham, A. M. & Sommeria, J. 2005 Decaying grid turbulence in a strongly stratified fluid. *J. Fluid Mech.* **522**, 1–33.

Riley, J. J., Metcalfe, R. W. & Weissman, M. A. 1981 Direct numerical simulation of homogeneous turbulence in density-stratified fluids. In *Proc. Conf. on Nonlinear Properties of Internal Waves* (ed. J. B. West), pp. 79–112. American Institute of Physics.

Smith, L. M. & Waleffe, F. 1999 Transfer of energy to two-dimensional large scale in forced, rotating three-dimensional turbulence. *Phys. Fluids* **11**, 1608–1622.

Smith, L. M. & Waleffe, F. 2002 Generation of slow large scales in forced rotating stratified turbulence. *J. Fluid Mech.* **451**, 145–168.

de Verdiere, A. C. 1980 Quasi-geostrophic turbulence in a rotating homogeneous fluid. *Geophys. Astrophys. Fluid Dyn.* **15**, 213–251.

Waleffe, F. 1993 Inertial transfert in the helical decomposition. *Phus. Fluids* A **5**, 677–685.